JOURNAL OF SYNCHROTRON RADIATION
ISSN 1600-5775

Angular dispersion enhanced prebunch for seeding ultrashort and coherent EUV and soft X-ray free-electron laser in storage rings

Xiaofan Wang,[a,b] Chao Feng,[a]* Tao Liu,[a] Zhen Zhang,[c] Cheng-Ying Tsai,[d] Juhao Wu,[c] Chuan Yang[e] and Zhentang Zhao[a]*

[a]Shanghai Institute of Applied Physics, Chinese Academy of Sciences, Shanghai 201800, China, [b]University of Chinese Academy of Sciences, Beijing 100049, China, [c]SLAC National Accelerator Laboratory, Menlo Park, CA 94025, USA, [d]Huazhong University of Science and Technology, Wuhan 430074, China, and [e]University of Science and Technology of China, Hefei 230026, China. *Correspondence e-mail: fengchao@sinap.ac.cn, zhaozhentang@sinap.ac.cn

Received 29 November 2018
Accepted 21 February 2019

Edited by I. Lindau, SLAC/Stanford University, USA

Keywords: angular dispersion; storage rings; free-electron lasers; extreme-ultraviolet (EUV); ultrashort; prebunching; high-harmonic bunching; radiation saturation length.

Prebunching is an effective technique to reduce the radiation saturation length and to improve the longitudinal coherence and output stability in storage-ring-based free-electron lasers (FELs). A novel technique is proposed which uses angular dispersion to enhance the high-harmonic bunching with very small laser-induced energy spread. This technique can effectively reduce the radiation saturation length without significantly reducing the peak power of the FEL. Numerical simulations demonstrate that this technique can be used for the generation of 100 MW scale level, fully temporal coherent femtosecond extreme-ultraviolet and soft X-ray radiation pulses through a 10 m-long undulator based on a diffraction-limited storage ring.

1. Introduction

Synchrotron light sources are a mature and reliable technology that can deliver radiation from infrared to soft X-rays with high beam stability, repetition rates and availability of multiple beamlines (Kim *et al.*, 2017; Zhao, 2010). About 10 ps radiation pulses can be generated to study the structure of matter from the molecular to the atomic scale. Linac-based free-electron lasers (FELs) have been a complementary tool to synchrotron light sources for the generation of radiation pulses with high peak brilliance, high degree of coherence and ultrafast resolution (Feng & Deng, 2018). Combining these two techniques has been of remarkable interest to the accelerator community (Kim *et al.*, 1985; Murphy & Pellegrini, 1985; Cornacchia *et al.*, 1986; Nuhn *et al.*, 1992; Huang *et al.*, 2008; Dattoli *et al.*, 2012; Cai *et al.*, 2013; Agapov, 2015; Di Mitri & Cornacchia, 2015; Labat *et al.*, 2007, 2009; De Ninno *et al.*, 2008; Khan *et al.*, 2013; Xiang & Wan, 2010).

The self-amplified spontaneous emission (SASE) mechanism (Kondratenko & Saldin, 1980; Bonifacio *et al.*, 1984) has been considered for storage-ring-based FELs (Kim *et al.*, 1985; Murphy & Pellegrini, 1985; Cornacchia *et al.*, 1986; Nuhn *et al.*, 1992; Huang *et al.*, 2008; Dattoli *et al.*, 2012; Cai *et al.*, 2013; Agapov, 2015; Di Mitri & Cornacchia, 2015). The SASE output is typically characterized by excellent spatial but limited temporal coherence. The spontaneous radiation is amplified by instability in the SASE mechanism, leading to large shot-to-shot fluctuations and a relatively long undulator length (typically 100 m) to reach saturation of the FEL. Long undulators would undoubtedly limit the capacity of the storage rings, as rings usually do not have sufficient space to accommodate very long undulators.

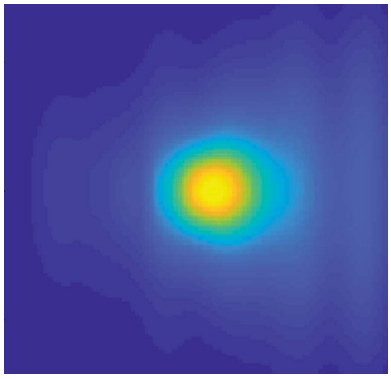

Table 1
Nominal electron-beam parameters used in the simulations.

Beam energy	1.5 GeV
Relative energy spread	0.15%
Peak current (I_0)	300 A
Geometric horizontal emittance	0.2 nm rad
Geometric vertical emittance	2 pm rad

Prebunching is an effective technique to overcome some of the present limitations of storage-ring-based SASE FELs. Prebunching means that the electron beam has been prebunched on the scale of the resonant wavelength, prior to the injection of the radiator (Schnitzer & Gover, 1985). Prebunching would not only shorten the saturation length substantially but also improve the longitudinal coherence and output stability (Freund *et al.*, 2012; Jia, 2017). Prebunching normally relies on frequency up-conversion schemes, which generally adopt the techniques of optical-scale manipulation of the electron-beam phase space with external coherent laser sources. Massive bunch manipulation techniques have been proposed to produce prebunched electrons, *e.g.* coherent harmonic generation (CHG) (Girard *et al.*, 1984; Yu, 1991; Yu *et al.*, 2000), echo-enabled harmonic generation (EEHG) (Stupakov, 2009; Xiang & Stupakov, 2009) and phase-merging enhanced harmonic generation (PEHG) (Deng & Feng, 2013; Feng *et al.*, 2014).

To illustrate that prebunching has the advantage of miniaturizing facility, here we compare the peak power as a function of propagation distance in the undulator with different initial energy spread for SASE and prebunching cases. Simulations were performed using *GENESIS* (Reiche, 1999). For the prebunching cases, the initial bunching factors for the entire bunch are directly set in *GENESIS*. Representative parameters of diffraction-limited storage rings are summarized in Table 1. The bunch peak current is set as 300 A here (Xiang & Wan, 2010; Ding *et al.*, 2013). The radiation wavelength is 13.5 nm and the undulator period is 3 cm.

Simulation results are shown in Fig. 1. SASE (ES = 0.05%) means FEL radiation generated from electrons with an energy spread of 0.05%. PreBunch (IB = 0.1) means FEL radiation generated from prebunched electrons with an initial bunching factor of 0.1. As can be seen from Fig. 1, the prebunching cases result in substantial shortening of the saturation length, while keeping the approximate peak power with respect to SASE. It also shows that for either SASE or prebunching cases, in comparison with low energy-spread cases, large energy-spread cases have lower saturation power and longer saturation length. The energy spread in storage rings is typically 0.1% or larger. With this large energy spread, SASE typically requires a very long undulator to reach saturation. While for prebunched cases, strong coherent spontaneous emission at the initial radiation stage speeds up the laser-beam interaction, resulting in a much shorter saturation length.

CHG is the most representative mechanism for prebunching and has been successfully applied to storage rings to generate ultrashort and coherent radiation (Ortega, 1986; Prazeres *et al.*, 1988, 1991; Labat *et al.*, 2007, 2009;

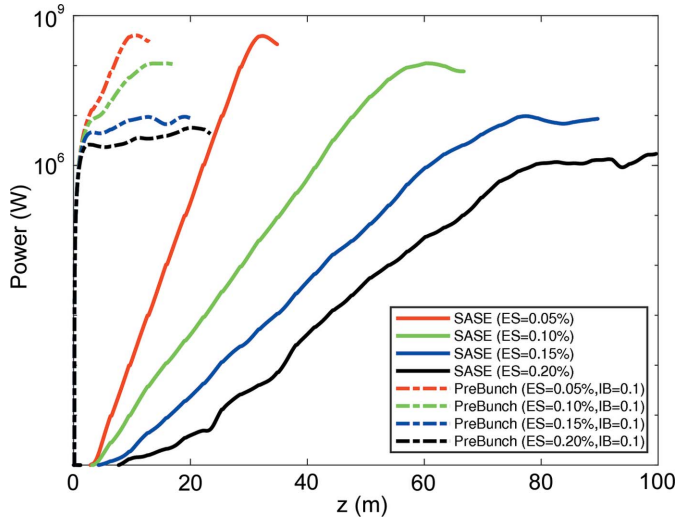

Figure 1
Peak power as a function of propagation distance in the undulator with different initial energy spread. SASE and prebunched cases are compared here. SASE (ES = 0.05%) means FEL radiation generated from electrons with an energy spread of 0.05%; PreBunch (IB = 0.1) means FEL radiation generated from prebunched electrons with an initial bunching factor of 0.1.

De Ninno *et al.*, 2008; Khan *et al.*, 2013). Generating microbunching at the nth harmonic of the seed laser requires the energy-modulation amplitude to be approximately n times larger than the initial beam energy spread, whereas large energy modulation is definitely not the best option, as can be seen from Fig. 1. EEHG and PEHG can significantly reduce the required energy modulation for ultra high harmonic generation. However, the laser-induced energy spread seems still too large for high-gain FEL in storage rings. Later, a mechanism which can introduce bunching to the electron beam with small energy modulation is proposed (Xiang & Wan, 2010). Compared with previous coherent harmonic generation methods, this scheme relies on the angular modulation instead of the energy modulation. However, the indispensable UV seed laser with TEM_{01} mode is difficult to obtain. Besides, complex lattice design would bring realistic difficulties.

In this work, a promising scheme is proposed, which uses angular dispersion to enhance the prebunching with very small laser-induced energy modulation. This technique can effectively reduce the radiation saturation length without significantly reducing the peak power. Numerical simulations demonstrate that this technique can be used for the generation of 100 MW scale level, fully temporal coherent femtosecond extreme-ultraviolet (EUV) and soft X-ray radiation through a 10 m-long undulator in a storage-ring free-electron laser.

The paper is organized as follows: the schematic layout is introduced in Section 2; theoretical derivation and comparison with existing schemes are described in Sections 2.1 and 2.2, respectively; three-dimensional simulations for the generation of ring-based EUV radiation with realistic parameters based on the proposed scheme are provided in Section 3; and finally we summarize the results in Section 4.

2. Schematic layout

Fig. 2 illustrates the schematic layout of the proposed scheme and longitudinal beam phase-space evolution within one seed-laser wavelength region. Frenet–Serret coordinates are given here, where x, y and z represent the horizontal, vertical and longitudinal coordinates, respectively. The electron beam is regulated in the z–y plane. The initial longitudinal phase space is shown in Fig. 2(a). Firstly, the electron beam interacts with the wavefront tilted seed laser 'seed light' in a short undulator, called a modulator, in which a tilted small sinusoidal energy modulation on the seed-laser wavelength scale will be imprinted onto the phase space of the electron beam. Then the phase space becomes Fig. 2(b). This energy modulation is then transformed into an associated density modulation by a dipole magnet, shown in Fig. 2(c). Taking advantage of the fact that the density modulation reflects as Fourier components at high harmonics of the seed frequency, intense radiation at shorter wavelengths shall be generated at the radiator.

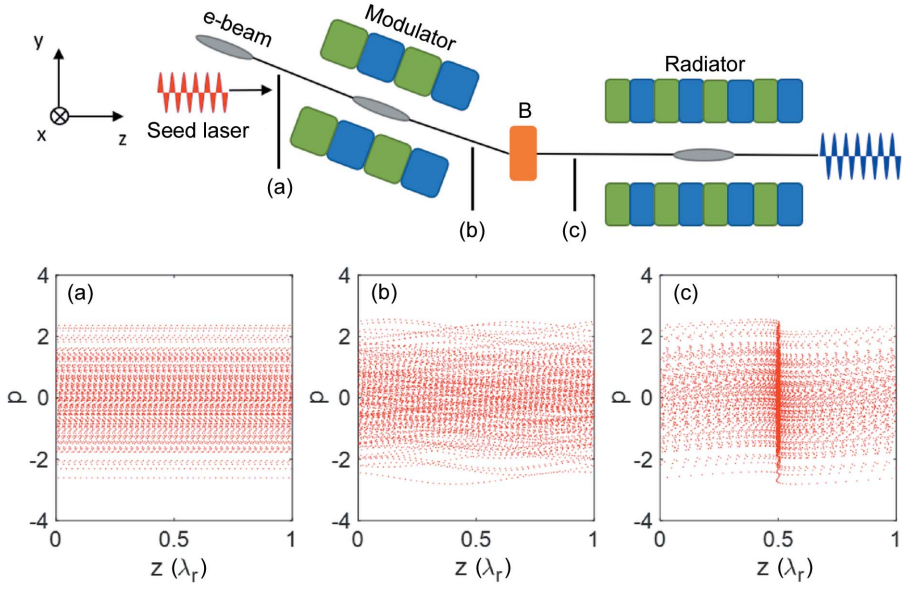

Figure 2
Schematic layout of the beamline for the proposed scheme and the longitudinal phase-space evolution: (a) the initial phase space; (b) the phase space at the exit of the modulator; and (c) the phase space at the entrance of the radiator.

The density modulation of the electron beam that contains high-harmonic components is usually quantified by the bunching factor. In the following, we will derive the expression of the bunching factor and analytically compare the proposed scheme with existing schemes.

2.1. Theoretical derivation

To briefly demonstrate the principle of the proposed scheme, we adopt the simplified 4 × 4 dimensional linear beam transport matrix in the y–z plane, *i.e.* (y, y', z, δ), where y and z are the vertical and longitudinal coordinates, $y' = \mathrm{d}y/\mathrm{d}z$ is the vertical divergence and $\delta = (\gamma - \gamma_0)/\gamma_0$ is the dimensionless energy deviation with respect to the reference particle (Chao *et al.*, 2013).

The electron interacts with a wavefront tilted seed laser intersecting at an angle of θ relative to the beam-propagation direction in the modulator and obtains an energy change. The electric field of the laser is independent of y. The energy modulation can be simply written as (Feng *et al.*, 2015)

$$\delta_1 = \delta_0 + O\sin(k_s z + \theta k_s y), \tag{1}$$

where k_s is the wavenumber of the seed light and $O = \Delta\gamma/\gamma_0$ is the induced beam energy change by laser-beam interaction. According to the Panofsky-Wenzel theorem (Panofsky & Wenzel, 1956), $(\partial/\partial y)(\Delta\gamma/\gamma) = (\partial\Delta y')/\partial z$, there will be an angular modulation,

$$y_1' = y_0' + O\,\theta\sin(k_s z + \theta k_s y). \tag{2}$$

Considering electrons in one seed wavelength range, the electron beam around the positive zero crossing of the seed laser gets an almost linear energy chirp $h = k_s O$. Therefore the energy change of the electron can be written as $\delta_1 \simeq \delta_0 + h(z + \theta y)$ and the angular change of the electron can be written as $y_1' = y_0' + h\theta(z + \theta y)$. Then the corresponding transport matrix of the electron beam for this modulation section can be derived as

$$R_M = \begin{pmatrix} 1 & 0 & 0 & 0 \\ h\theta^2 & 1 & h\theta & 0 \\ 0 & 0 & 1 & 0 \\ h\theta & 0 & h & 1 \end{pmatrix}. \tag{3}$$

After the modulator, the energy modulation is converted into density modulation by a dipole magnet. Under the thin-lens approximation, the transport matrix of a dipole is

$$R_B = \begin{pmatrix} 1 & L_b & 0 & \eta \\ 0 & 1 & 0 & -b \\ b & \eta & 1 & 0 \\ 0 & 0 & 0 & 1 \end{pmatrix}, \tag{4}$$

where L_b represents R_{12} in the matrix, and b and η are the bending angle and dispersion of the dipole, respectively. Then the transport matrix for the whole beamline is

$$R = R_B R_M = \begin{pmatrix} 1 + h\theta\eta + h\theta^2 L_b & L_b & h(\eta + \theta L_b) & \eta \\ h\theta(\theta - b) & 1 & h(\theta - b) & -b \\ b + h\theta^2\eta & \eta & 1 + h\theta\eta & 0 \\ h\theta & 0 & h & 1 \end{pmatrix}. \tag{5}$$

To enhance the high-harmonic bunching, the electrons should merge into the same longitudinal position to the greatest extent, which means the items in the third row of equation (5)

should be as small as possible. Therefore, we can obtain the optimization conditions of the proposed scheme:

$$\theta = b, \qquad 1 + h\theta\eta = 0. \tag{6}$$

Once these conditions are satisfied, the longitudinal position of the electron after the density modulation can be written as

$$z_1 = \eta y'. \tag{7}$$

It should be emphasized that equations (3)–(7) refer to a small (∼20%) portion of the electron beam. However, the bunching of the entire bunch is primarily determined by the aggregation degree of this portion of the electrons. We can tell from equation (7) that the high-harmonic bunching factor will be determined by the product of η and the initial vertical beam divergence $\sigma_{y'}$. Considering the sinusoidal modulation for the whole beam, a more solid derivation of the proposed scheme gives the straightforward bunching factor as

$$b_n = \exp\left[-\frac{(nk_s\eta\sigma_{y'})^2}{2}\right] J_n(-nh\theta\eta), \tag{8}$$

where J_n is the nth order Bessel function.

In order to enhance the bunching factor for a given $\Delta\gamma$ in the proposed scheme, one can increase the beta function at the entrance of the proposed scheme to reduce σ_y' or increase the incidence angle θ to reduce as required the dispersion strength of the dipole magnet η. Although the balance between quantum excitation and radiation damping results in a relatively large energy spread in the storage ring, it nonetheless provides a beam with quite a low transverse emittance. The proposed technique makes full use of this feature and thus has the potential to significantly enhance the frequency up-conversion efficiency.

2.2. Comparison with existing schemes

To illustrate the advantages of the proposed scheme, we compared it with three existing schemes, *i.e.* CHG, EEHG and PEHG. The bunching factor at the nth harmonic of the CHG is given by (Yu, 1991):

$$b_n = \exp\left[-\frac{n^2B^2}{2}\right] J_n(-nAB), \tag{9}$$

where $A = \Delta\gamma/\sigma_\gamma$ is the energy-modulation amplitude, $B = (R_{56}k_s\sigma_\gamma)/\gamma$ is the dimensionless strength of the chicane, and k_s and R_{56} are the wavenumber of the seed light and the momentum compaction in the chicane, respectively. In the following discussion, the definitions of A and B are the same as those defined here.

The PEHG was proposed to improve the frequency up-conversion efficiency of the CHG. The bunching factor at the nth harmonic of the PEHG is given by (Deng & Feng, 2013):

$$b_n = \exp\left[-\frac{n^2T^2}{2}\right] \exp\left[-\frac{n^2(B+TD)^2}{2}\right] J_n(-nAB), \tag{10}$$

where T is the dimensionless gradient parameter of the transverse gradient undulator (TGU) and $D = (\eta\sigma_\gamma)/(\sigma_x\gamma)$ is the dimensionless dispersive strength in the horizontal. A previous study (Qi *et al.*, 2017) showed that the intrinsic beam divergence would decrease the phase-merging effect, leading to a lower bunching factor. For simplicity, the influence of intrinsic beam divergence on the bunching factor is ignored here, thus equation (10) indicates the best performance of PEHG.

Another effective way to achieve electron-beam bunching is the EEHG. The bunching factor at the ath harmonic of the EEHG is given by (Stupakov, 2009):

$$b_a = \sum_{n,m} \exp\left[-\frac{C^2}{2}\right] J_n(-CA_1) J_m(-aA_2B_2), \tag{11}$$

where $a = n + mK$ and $C = nB_1 + (n + mK)B_2$. Furthermore, A_1 and A_2 are the energy-modulation amplitudes of the first and second modulator, respectively, and B_1 and B_2 are the dimensionless strengths of the first and second chicane, respectively.

From the above discussion, we can plot modulation depth as a function of bunching factor at the 20th harmonic for the above three and proposed schemes based on equations (9)–(11), as shown in Fig. 3. One can see that for either CHG, PEHG or EEHG the energy-modulation amplitude should be at least 2 to achieve a bunching factor of 0.1 for the 20th harmonic. This would undoubtedly boost the energy spread in storage rings, resulting in a significant reduction of the peak power. Also, the saturation length will not decrease much. For the proposed scheme, however, the bunching factor is insensitive to the modulation depth. Therefore a very small energy-modulation amplitude can generate a large bunching factor. On the whole, the proposed scheme could effectively reduce the saturation length while almost not changing the peak power.

It should be stressed that a recently proposed technique (Feng & Zhao, 2017) could also imprint strong coherent microbunching on the electron beam with a small laser-induced energy spread. Mathematically, the energy-modulation depths of these two schemes could reach the same

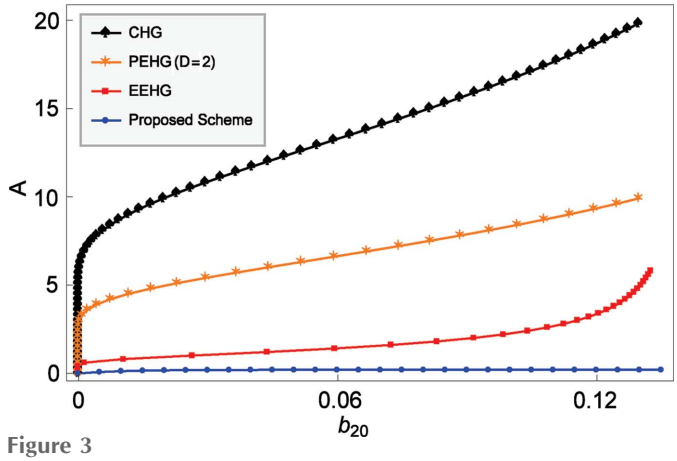

Figure 3
Modulation depth as a function of bunching factor at the 20th harmonic of CHG, PEHG, EEHG and the proposed scheme. The dimensionless dogleg strength in PEHG is set to be 2. Further increase of the dogleg strength can decrease the modulation depth. For EEHG, only the first modulation depth is shown here.

level (∼0.2). However, these two schemes adopt different implementations. With only a dipole and a short modulator, the lattice layout for the proposed scheme here is more simplified to achieve similar results.

3. 3D simulations for the generation of intense EUV radiation

To illustrate a possible application with realistic parameters and show the parameter-optimization method of the proposed scheme, three-dimensional simulations are carried out based on the beam parameters in Table 1.

The modulation process was simulated with a three-dimensional algorithm based on the fundamentals of electrodynamics when considering the appearance of the electromagnetic fields of a wavefront tilted seed laser and the magnetic fields of the modulator. It is assumed that the r.m.s. intrinsic beam size at the entrance of the modulator is σ_x = 45 µm and σ_y = 25 µm. The modulator is composed of a four-period undulator magnet with 2.1 cm period, 7.5 mm gap, and a K value of 1.45. A round laser pulse with a duration of 100 fs FWHM, a central wavelength of 270 nm, a peak power of 700 GW and an incident angle of 5 mrad is adopted. Since the laser is obliquely incident, the center of the laser field gradually deviates from the center of the electron beam as it passes through the undulator. The deviation distance between the seed-laser center and electron-beam center is equal to the product of the modulator length and the seed-laser incident angle, which is 0.42 mm in this case. This parameter is approximately ten times larger than the transverse size of the electron beam. Therefore, the seed-laser spot size is mainly determined by the deviation distance. To fully cover the electron beam, the transverse size of the laser waist is set to 0.84 mm. Interacting with electrons in the modulator, this laser pulse will produce a peak amplitude of energy modulation of ∼0.9 MeV (*i.e.* 0.2 times of tinitial energy spread). In addition to energy modulation, angular modulation is also induced in the modulator. The energy and angle are both modulated on the scale of the seed-laser wavelength. Besides, the appearances of the energy and divergence distribution after modulation are the same. Here we illustrate the vertical divergence distribution after the laser-beam interaction in Fig. 4. One can see that the divergence distribution is tilted with an inclined angle of 5 mrad and the longitudinal distance between the two modulation peaks is exactly the wavelength of one seed laser. These results are consistent with equation (2).

After the electron beam traverses a dipole magnet or a transport section with a matrix of $R_{16} = -0.0312$ m, $R_{51} = 0.005$ and $R_{56} = -4$ µm, it will enter into the radiator. Introducing R_{56} by the dipole or a chicane magnet would make the electron beam under-compressed, lowering the initial bunching factor while enhancing the final radiation peak power. Simulations for the radiation process were performed by *GENESIS* (Reiche, 1999). The period length of the radiator is 3 cm with a K value of about 3.7. The FODO structure is well designed to have the following Twiss parameters at the entrance of the FODO cell: β_x = 10.5 m, β_y = 1.9 m, $\alpha_x = -1.9$, α_y = 0.37. With these parameters, the resultant beam size is σ_x = 46 µm and σ_y = 1.95 µm in the SASE case. In the proposed case, the geometric vertical emittance is boosted to 0.2 nm because of modulation. Then the beam size is σ_x = 46 µm and σ_y = 20 µm.

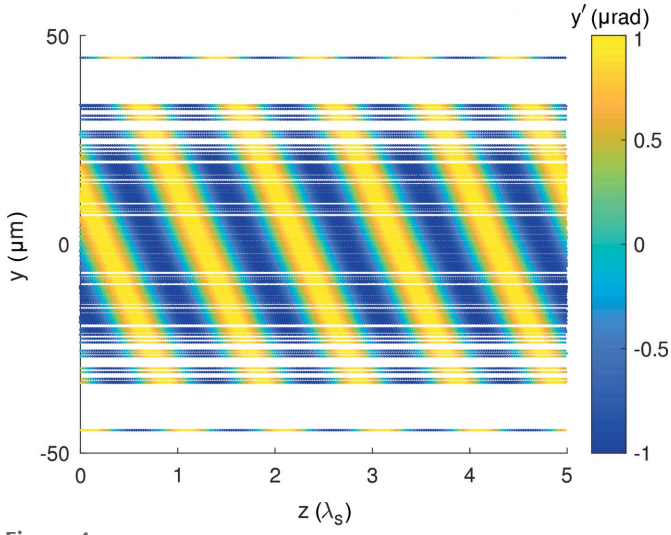

Figure 4
Three-dimensional simulation result of the vertical divergence distribution after the laser-beam interaction.

The evolutions of the bunching factor and radiation peak power for SASE and the proposed scheme at the 20th harmonic are shown in Fig. 5. The dispersion induced by the undulator becomes apparent for electrons with 0.15% energy spread. Therefore, for the proposed scheme the under-compressed prebunch would subsequently become fully compressed as it propagates in the undulator. This can be seen in Fig. 5(*a*), where the bunching factor increases from 0.04 to 0.38 within an undulator length of 10 m. Then coherent radiation scales as n_e^2 (where n_e is the electron-beam density),

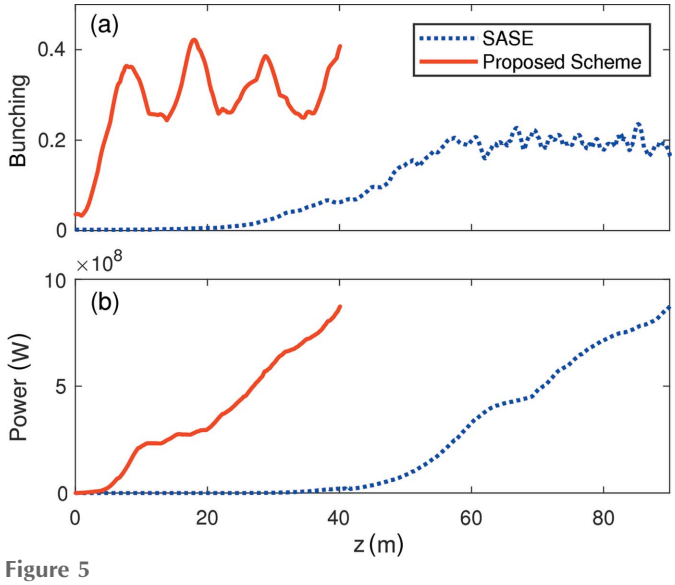

Figure 5
Evolution of (*a*) the bunching factor and (*b*) the peak power at the 20th harmonic (13.5 nm) as a function of the radiator distance of SASE (blue dashed line) and the proposed scheme (red solid line), respectively.

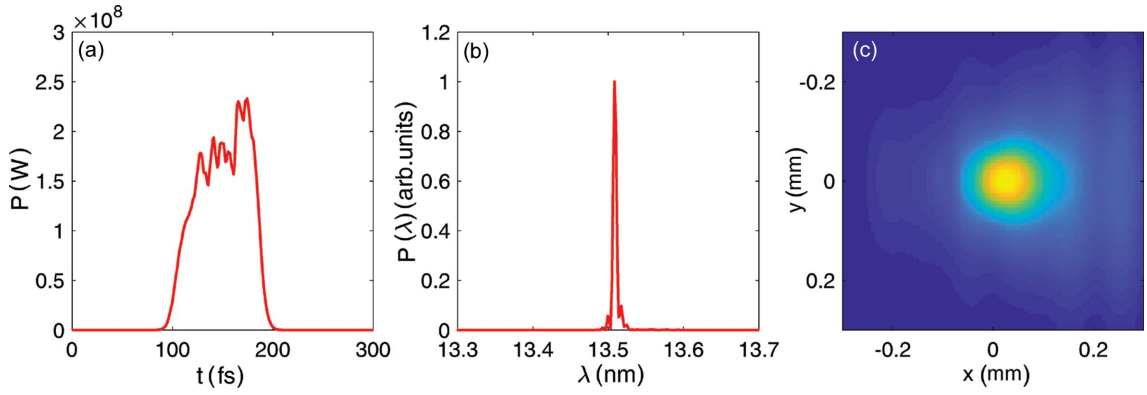

Figure 6
FEL performance of the 20th harmonic at z = 10 m: (a) output radiation pulses; (b) output spectra and (c) transverse distribution of radiation pulses.

which would be emitted by the well prebunched electrons. The radiation reaches the saturation region at an undulator length of 10 m and ∼200 MW of peak power can be generated. However, driven by FEL instability, SASE needs a 60 m or longer undulator to approach power of a comparable level. Hence, compared with SASE, the proposed scheme shows remarkable performance when the undulator is short. It is also shown that the peak power emitted by the electrons scales as n_e^2 again after a undulator length of 20 m for the proposed scheme, which is typical of strong superradiant behavior (Bonifacio *et al.*, 1989), the superradiant regime showing continuous energy extraction from the electron pulse.

Fig. 6 shows the output radiation pulses, output spectra and transverse distribution of the 20th harmonic radiation pulses for the proposed scheme at z = 10 m. One can see from Fig. 6(a) that ∼60 fs FWHM laser pulses could be generated. Furthermore, one can see from Fig. 6(b) that the spectral bandwidth at 10 m for the proposed scheme is close to the Fourier transform-limited bandwidth. Therefore, the radiation pulse is almost fully coherent. As can be seen from Fig. 6(c), radiation pulses are approximately round in the transverse plane. This is because the geometric vertical emittance is boosted to the value of the geometric horizontal emittance during the modulation process.

In Fig. 6(a), a relatively high spiking shows up in the leading region. This is because there is always a trailing region of the electron beam in which slippage effects give rise to spiking behavior in the head of the radiation pulse. The radiation pulses constantly interact with the fresh bunch in the head region and the energy is extracted from the electrons in a continuous way, leading to a spiking behavior (see Fig. 7). The heading spiking has an approximate 8 fs FWHM temporal structure at z = 40 m, which may be very useful for experiments investigating ultrafast phenomena.

4. Conclusions

In this work, we have proposed a novel technique, which can introduce prebunching to the electron beam. This beam-manipulation technique uses a wavefront tilted laser to modulate the electron beam. Relying on angular modulation instead of energy modulation, this technique could enhance

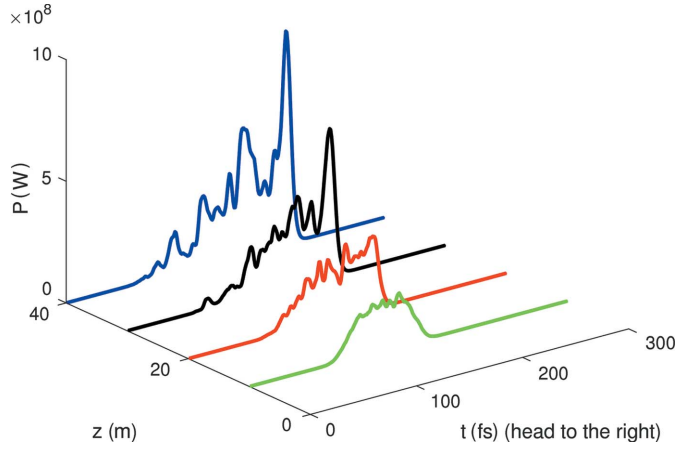

Figure 7
Output radiation pulses of the 20th harmonic at different radiation distances.

high-harmonic bunching with a very small laser-induced energy spread. With a simple setup of a short modulator and a dipole magnet, this technique is very dexterous for implementation in existing facilities.

In the three-dimensional simulations, 200 MW fully temporal coherent EUV radiation pulses with a duration of 60 fs FWHM are generated through a 10 m-long undulator. This is an unprecedented performance. This technique effectively reduces the radiation saturation length without significantly reducing the peak power with respect to storage-ring-based SASE FELs. Although EUV radiation pulses are generated in this work, this technique possesses the ability to further extend the output wavelength range towards soft X-rays. The peak power of the seed laser is 700 GW in our case. This would be a primary limitation for the repetition rate in storage-ring-based FELs. It is found that the energy-modulation depth increases as the incident angle decreases. Therefore, under the resonant condition, for a given modulation depth, directly reducing the incidence angle would significantly reduce the intensity of the seed laser. The laser spot size is proportional to the incident angle. Reducing the incidence angle would also lower the laser spot size, which increases the laser intensity. Increasing the modulation length

is not working here because the laser spot size is proportional to the modulation length. In addition, we can use an elliptical cross-section seed laser. The laser size in the vertical direction is mainly determined by the deviation distance; however, in the horizontal direction, the laser size is determined by the electron-beam size. The deviation distance is an order of magnitude larger than the beam size. Therefore, the adoption of elliptical rather than circular cross-section seed lasers can reduce laser power by one order of magnitude to ∼70 GW. Another possible solution is inserting a quadrupole magnet in front of this scheme. By elaborately setting the parameters of each component, this method could achieve the same bunching factor with a smaller energy-modulation depth. Then further lowering the required energy-modulation amplitude.

The laser–electron interaction would slightly increase the energy spread and boost the vertical emittance of the electron beam. This part of the electron beam may not be conducive to the generation of synchrotron radiation. However, the interaction only happens in 100 fs of the bunch, a tiny fraction of the 10 ps bunch length that is typical in a storage ring. Then the proposed technique may not adversely affect the other beamlines (Schoenlein *et al.*, 2000).

Steady state microbunching (SSMB) is a promising technique to generate high average radiation power in storage rings (Ratner & Chao, 2010; Ratner & Chao, 2011). Preliminary study shows that the proposed technique has the feasibility to be used in reversible SSMB. Further investigations of this topic are ongoing.

Acknowledgements

The authors are deeply grateful to Alex Chao (SLAC) for providing the vision and guidance during the proposal of the scheme. We would also like to thank Bocheng Jiang (Shanghai Institute of Applied Physics – SINAP) and Guanqun Zhou (Institute of High Energy Physics – IHEP) for helpful discussions and useful comments related to the work presented here.

Funding information

Funding for this research was provided by: National Nature Science Foundation of China (grant No. 11475250; grant No. 11605277); National Key Research and Development Program of China (grant No. 2016YFA0401901) and Youth Innovation Promotion Association CAS (grant No. 2015209). The support provided by China Scholarship Council (CSC) during a visit of Xiaofan Wang to SLAC is acknowledged.

References

Agapov, I. (2015). *Nucl. Instrum. Methods Phys. Res. A*, **793**, 35–40.
Bonifacio, R., McNeil, B. & Pierini, P. (1989). *Phys. Rev. A*, **40**, 4467–4475.
Bonifacio, R., Pellegrini, C. & Narducci, L. M. (1984). *Opt. Commun.* **50**, 373–378.
Cai, Y., Ding, Y., Hettel, R., Huang, Z., Wang, L. & Xiao, L. (2013). *Synchrotron Radiat. News*, **26**(3), 39–41.
Chao, A. W., Mess, K. H., Tigner, M. & Zimmerman, F. (2013). *Handbook of Accelerator Physics and Engineering.* 2nd ed. Singapore: World Scientific.
Cornacchia, M., Bisognano, J., Chattopadhyay, S., Garren, A., Halbach, K., Jackson, A., Kim, K. J., Lancaster, H., Peterson, J., Zisman, M. S., Pellegrini, C., Zisman, M. S. (1986). *Nucl. Instrum. Methods Phys. Res. A*, **250**, 57–63.
Dattoli, G., Palma, E. D., Petralia, A. & Rau, J. V. (2012). *IEEE J. Quantum Electron.* **48**, 1259–1264.
Deng, H. & Feng, C. (2013). *Phys. Rev. Lett.* **111**, 084801.
De Ninno, G., Allaria, E., Coreno, M., Chowdhury, S., Curbis, F., Danailov, M., Diviacco, B., Ferianis, M., Karantzoulis, E., Longhi, E., Pinayev, I. V., Spezzani, C., Trovò, M. & Litvinenko, V. N. (2008). *Phys. Rev. Lett.* **100**, 104801.
Di Mitri, S. & Cornacchia, M. (2015). *New J. Phys.* **17**, 113006.
Ding, Y., Baxevanis, P., Cai, Y., Huang, Z. & Ruth, R. D. (2013). *Proc. IPAC2013*, Shanghai, China, pp. 2286–2288. WEPWA075.
Feng, C. & Deng, H. (2018). *Nucl. Sci. Tech.* **29**, 160.
Feng, C., Deng, H., Wang, D. & Zhao, Z. (2014). *New J. Phys.* **16**, 043021.
Feng, C., Xiang, D., Deng, H., Huang, D., Wang, D. & Zhao, Z. (2015). *Opt. Express*, **23**, 14993–15002.
Feng, C. & Zhao, Z. (2017). *Sci. Rep.* **7**, 4724.
Freund, H. P., Nguyen, D. C. & Carlsten, B. (2012). *Phys. Rev. ST Accel. Beams*, **15**, 030704.
Girard, B., Lapierre, Y., Ortega, J. M., Bazin, C., Billardon, M., Elleaume, P., Bergher, M., Velghe, M. & Petroff, Y. (1984). *Phys. Rev. Lett.* **53**, 2405–2408.
Huang, Z., Bane, K., Cai, Y., Chao, A., Hettel, R. & Pellegrini, C. (2008). *Nucl. Instrum. Methods Phys. Res. A*, **593**, 120–124.
Jia, Q. (2017). *Phys. Rev. Accel. Beams*, **20**, 070702.
Khan, S., Bahnsen, F., Cramm, S., Döring, S., Grewe, J., Höner, M., Huck, H., Huck, M., Molo, R., Plucinski, L., Schick, A., Schneider, C. M. & Ungelenk, P. (2013). *Synchrotron Radiat. News*, **26**(3), 25–29.
Kim, K.-J., Bisognano, J., Garren, A., Halbach, K. & Peterson, J. (1985). *Nucl. Instrum. Methods Phys. Res. A*, **239**, 54–61.
Kim, K.-J., Huang, Z. & Lindberg, R. (2017). *Synchrotron Radiation and Free-Electron Lasers: Principles of Coherent X-ray Generation.* Cambridge University Press.
Kondratenko, A. & Saldin, E. (1980). *Part. Accel.* **10**, 207–216.
Labat, M., Hosaka, M., Mochihashi, A., Shimada, M., Katoh, M., Lambert, G., Hara, T., Takashima, Y. & Couprie, M. (2007). *Eur. Phys. J. D*, **44**, 187–200.
Labat, M., Hosaka, M., Shimada, M., Yamamoto, N., Katoh, M. & Couprie, M. (2009). *Phys. Rev. Lett.* **102**, 014801.
Murphy, J. B. & Pellegrini, C. (1985). *Nucl. Instrum. Methods Phys. Res. A*, **237**, 159–167.
Nuhn, H.-D., Tatchyn, R., Winick, H., Fisher, A. S., Gallardo, J. C. & Pellegrini, C. (1992). *Nucl. Instrum. Methods Phys. Res. A*, **319**, 89–96.
Ortega, J. (1986). *Nucl. Instrum. Methods Phys. Res. A*, **250**, 203–211.
Panofsky, W. & Wenzel, W. (1956). *Rev. Sci. Instrum.* **27**, 967.
Prazeres, R., Guyot-Sionnest, P., Ortega, J., Jaroszynski, D., Billardon, M., Couprie, M., Velghe, M. & Petroff, Y. (1991). *Nucl. Instrum. Methods Phys. Res. A*, **304**, 72–76.
Prazeres, R., Ortega, J., Bazin, C., Bergher, M., Billardon, M., Couprie, M., Velghe, M. & Petroff, Y. (1988). *Nucl. Instrum. Methods Phys. Res. A*, **272**, 68–72.
Qi, Z., Feng, C., Deng, H., Liu, B. & Zhao, Z. (2017). *Nucl. Instrum. Methods Phys. Res. A*, **875**, 119–124.
Ratner, D. F. & Chao, A. W. (2010). *Phys. Rev. Lett.* **105**, 154801.
Ratner, D. F. & Chao, A. W. (2011). Technical Report SLAC-PUB-14718. SLAC National Accelerator Laboratory, Menlo Park, CA, USA.
Reiche, S. (1999). *Nucl. Instrum. Methods Phys. Res. A*, **429**, 243–248.
Schnitzer, I. & Gover, A. (1985). *Nucl. Instrum. Methods Phys. Res. A*, **237**, 124–140.

Schoenlein, R., Chattopadhyay, S., Chong, H., Glover, T., Heimann, P., Shank, C., Zholents, A. & Zolotorev, M. (2000). *Science*, **287**, 2237–2240.
Stupakov, G. (2009). *Phys. Rev. Lett.* **102**, 074801.
Xiang, D. & Stupakov, G. (2009). *Phys. Rev. ST Accel. Beams*, **12**, 030702.
Xiang, D. & Wan, W. (2010). *Phys. Rev. Lett.* **104**, 084803.
Yu, L. H. (1991). *Phys. Rev. A*, **44**, 5178–5193.
Yu, L. H., Babzien, M., Ben-Zvi, I., DiMauro, L., Doyuran, A., Graves, W., Johnson, E., Krinsky, S., Malone, R., Pogorelsky, I., Skaritka, J., Rakowsky, G., Solomon, L., Wang, X. J., Woodle, M., Yakimenko, V., Biedron, S. G., Galayda, J. N., Gluskin, E., Jagger, J., Sajaev, V. & Vasserman, I. (2000). *Science*, **289**, 932–935.
Zhao, Z. (2010). *Rev. Accl. Sci. Tech.* **03**, 57–76.